Applied Ocean Research 166 (2026) 104907

Contents lists available at ScienceDirect

Applied Ocean Research

journal homepage: www.elsevier.com/locate/apor

Research paper

Energy efficient formation control of multi vessel systems via hydrodynamics aware configuration optimization

Xin Xiong, Rudy R. Negenborn, Yusong Pang *

Delft University of Technology, Department of Maritime and Transport Technology, Delft, The Netherlands

ARTICLE INFO

Keywords:
Multi vessel systems
Model predictive control
Ship to ship interaction
Kelvin wave interference
Energy efficient control

ABSTRACT

Existing studies on multi-vessel formations rarely combine physically based models of ship–ship hydrodynamic interaction with online formation control, so that energy benefits are typically assessed offline or only approximated through artificial potentials. This paper addresses this gap by embedding a reduced-order, hydrodynamics-aware resistance model into a hierarchical formation control framework for multi vessel systems. A three degree of freedom interaction model is incorporated into the cost function, enabling the supervisory controller to adaptively optimize inter ship spacing and formation geometry in a speed dependent and hydrodynamics aware manner. The lower level MPC ensures accurate trajectory tracking and stability under the guidance of the top level optimization. Four simulation studies are conducted to evaluate the proposed method. The platooning formation is first analyzed as a reference, followed by the triangular formation, which achieves balanced tracking performance and stability. The echelon formation is then examined, demonstrating significant energy savings in medium to high speed regimes while maintaining yaw stability. Finally, an unconstrained optimization scenario is explored, where the system autonomously adapts its geometry without prescribed patterns, revealing emergent energy efficient and stable arrangements across different speed ranges. Results show that the proposed approach not only reduces resistance and improves energy efficiency but also enhances formation adaptability and robustness under varying operating conditions. These findings provide new insights into hydrodynamics aware cooperative control and the development of energy conscious fleet management strategies for future maritime transportation.

1. Introduction

Driven by the expansion of global maritime transport and escalating fuel costs, the shipping industry has placed greater emphasis on achieving higher energy efficiency and sustainable operations (Chen et al., 2019). Multi vessel cooperative control has emerged as a novel strategy, allowing vessels to form coordinated formations that leverage wake effects and ship to ship interactions to decrease navigational resistance and realize energy savings (Dong et al., 2022b). Drawing inspiration from collective behaviors in nature, such as fish schooling (Li et al., 2020), bird flocking (Andersson and Wallander, 2004), and duck formations (Yuan et al., 2021). This approach optimizes vessel positioning to harness wake induced advantages, thereby minimizing formation resistance and improving overall energy efficiency.

Multi vessel formation sailing is widely regarded as a promising strategy for improving energy efficiency. This theoretical potential has been substantiated by numerous simulation studies, which demonstrate that optimizing formation configurations, such as longitudinal spacing and relative positioning which can reduce total hydrodynamic resistance and propulsion energy consumption (Phillips et al., 2010a; Rattanasiri et al., 2012, 2015). However, despite these encouraging results, practical implementation remains limited. Most existing studies treat inter vessel distances as static optimization variables, overlooking the inherently nonlinear and dynamic nature of hydrodynamic interactions, which strongly influence both resistance and maneuverability (Xiong et al., 2024). Furthermore, as the fleet size increases, the complexity of coordination escalates due to additional requirements such as collision avoidance, communication delays, and actuator constraints. Current control frameworks often focus on single vessel optimization or basic formation maintenance, while the integration of hydrodynamic interaction models into real time control strategies for energy aware formation optimization remains largely unexplored.

1.1. Energy efficient sailing and hydrodynamic interactions

Existing literature identifies four primary approaches to enhancing energy efficiency in single vessels: hull optimization, operational

* Corresponding author.
E-mail addresses: X.Xiong-1@tudelft.nl (X. Xiong), R.R.Negenborn@tudelft.nl (R.R. Negenborn), Y.Pang@tudelft.nl (Y. Pang).

https://doi.org/10.1016/j.apor.2025.104907
Received 17 September 2025; Received in revised form 28 November 2025; Accepted 24 December 2025
Available online 16 January 2026

optimization, propulsion system optimization, and alternative energy combined with smart energy management. Hull optimization focuses on refining the hull shape and auxiliary structures to reduce navigational resistance. For instance, Yanuar et al. (2012) employing bubble drag reduction to minimize direct hull water contact and thereby lower frictional resistance. Moreover, optimizing the bow or overall hull form further contributes to resistance reduction (Wang et al., 2025; Xue et al., 2022). Operational optimization encompasses three main strategies: speed optimization (Yan et al., 2024; Li et al., 2023), route optimization (Vorkapić et al., 2021), and trim optimization (Wang et al., 2018). Propulsion system optimization primarily involves improving hybrid propulsion systems by exploring various power combinations to boost efficiency (Hong et al., 2024; Haseltalab and Negenborn, 2019; Nguyen and Chandar, 2023). Finally, alternative energy and smart energy management strategies seek to enhance ship energy efficiency by integrating renewable energy sources (Barone et al., 2024) with intelligent management systems (Karatuğ et al., 2024). Overall, these single-vessel energy-saving measures have achieved significant progress over the past decade, but their improvement potential is gradually approaching its limit. To further reduce energy consumption, it is necessary to explore novel approaches that can provide additional energy-saving potential.

Beyond single vessel strategies, increasing attention has been directed toward formation based energy saving in multi vessel systems. Inspired by natural collective behaviors such as bird flocking, fish schooling, and duck formations, researchers have demonstrated that optimized relative positioning can lead to substantial reductions in propulsion power through hydrodynamic cooperation. Simulation studies on Autonomous Underwater Vehicles (AUVs) (Phillips et al., 2012, 2010b) and Unmanned Surface Vessels (USVs) (Dong et al., 2022b) have shown that suitable inter vessel spacing significantly reduces resistance by leveraging wake effects and wave interference.

The fundamental mechanism driving these benefits lies in hydrodynamic interactions, including both wake exploitation and inter ship pressure field modulation. These effects have been analyzed in a variety of scenarios such as encounters, overtaking maneuvers, berthing, and at sea replenishment. For example, He et al. (2022a) used CFD simulations to evaluate formation induced resistance variations and confirmed the strong dependence of energy consumption on vessel arrangement. Zhou et al. (2015) investigated hydrodynamic interactions in constrained waterways and identified optimal fleet spacing to mitigate additional drag. Dong et al. (2022a) further revealed that sailing near the free surface alters wave patterns and maneuverability, which has direct implications for coordinated control.

Although hydrodynamic synergy in formations has been widely studied, existing methods predominantly rely on static or offline models and lack real time responsiveness to dynamic inter vessel interactions.

1.2. Formation control strategies and methods

Effective formation control in multi vessel systems hinges on both coordination strategies and advanced control algorithms. Various structural frameworks have been proposed, including the leader follower, Virtual Structure, and Behavior Based approaches. Among them, the leader follower paradigm remains the most prevalent, where a designated lead vessel defines the trajectory, and followers maintain predefined spatial relationships. To improve adaptability and robustness, enhancements such as sliding mode control, switching topologies (Dong et al., 2022c; Liu et al., 2021a), and event triggered role reassignment (Zhang et al., 2022) have been introduced. The virtual structure method models the entire formation as a rigid body to enforce coordinated motion (Dai et al., 2021; Fang et al., 2022), whereas behavior based models enable decentralized decision making using local interaction rules for tasks like collision avoidance and spacing maintenance (Mwaffo, 2024; Liu et al., 2021b).

Among control methods, MPC has emerged as a dominant framework due to its ability to handle multi objective optimization, enforce physical and operational constraints, and perform real time decision making. MPC optimizes a sequence of control inputs over a finite prediction horizon based on a system model, enabling anticipatory control that is especially well suited for formation scenarios requiring the simultaneous handling of hydrodynamic interactions, collision avoidance, and energy optimization. Studies have validated its effectiveness in COLREGS compliant collision avoidance (Hagen et al., 2022; He et al., 2022b) and cooperative operations, such as distributed towing systems (Du et al., 2021).

Zheng et al. (2014) applied MPC for autonomous vessel trajectory tracking, highlighting its constraint handling and tracking precision. Building on this, Zheng et al. (2016) proposed a fast ADMM based distributed MPC framework for cooperative waterborne AGVs, significantly reducing computational overhead. More recently, Tsolakis et al. (2024) incorporated traffic rules into MPC based trajectory optimization, showing that MPC can enforce COLREGs compliant navigation in complex, real world traffic environments.

To enhance scalability and fault tolerance, Distributed MPC (DMPC) has gained attention by decentralizing control across multiple vessels. This approach allows autonomous fleets to operate without reliance on a single central node, as shown in vessel train formations (Chen et al., 2018) and cooperative formation scenarios (Tang et al., 2022). While MPC based methods are powerful, they require accurate system modeling and significant computational resources.

Consequently, alternative data driven methods are increasingly being explored. Model Free Adaptive Control (MFAC) eliminates the need for explicit models, enabling fast adaptation in uncertain maritime environments (Wang et al., 2024). Reinforcement Learning (RL) approaches provide high adaptability and have shown promise when integrated with MPC to enhance formation control under dynamic and partially known conditions (Shang et al., 2023). Despite their strengths, RL methods often require extensive training data and may lack formal stability guarantees.

In summary, despite modeling and computational challenges, MPC remains the most promising framework for energy aware formation control of multi vessel systems. Its optimization based nature allows for transparent trade offs between energy consumption, trajectory accuracy, and safety constraints. Moreover, MPC provides a structured platform for integrating physical models, interaction aware objectives, making it highly suitable for real world deployment in increasingly complex maritime scenarios.

Despite extensive work on formation control and on hydrodynamic interactions between multiple ships, most existing control frameworks either neglect ship-to-ship interaction or embed them only implicitly through conservative safety margins or artificial potential fields. Energy savings from formation are then assessed offline, rather than used directly as an online control objective. Conversely, recent hydrodynamic studies on ship formations and ship-to-ship interactions provide detailed resistance and load characteristics as a function of spacing, layout, speed and water depth, but are rarely translated into real-time configuration decisions for multi-vessel control. This disconnect between hydrodynamic modeling and cooperative control motivates the present work.

1.3. Objective and contributions

This paper makes the following contributions.

1. A physically informed energy modeling framework is established for close-spacing formations. Total resistance is decomposed into frictional, pressure and wave-making components, and augmented with a Kelvin-wake inspired interaction term that depends on formation layout, longitudinal and lateral gaps, and Froude number. This yields an effective resistance model for the fleet that links configuration and speed to energy consumption.

2. A hierarchical, hydrodynamics-aware formation-control architecture is proposed. A supervisory decision layer optimizes configuration, inter-ship spacing and speed for energy efficiency, while a lower MPC layer enforces vessel dynamics, actuator limits and minimum-separation constraints. This separation keeps the online optimization small-scale and allows the use of standard quadratic programs in the MPC layer.
3. The decision layer employs a speed-dependent weighting scheme that balances energy efficiency and formation-keeping. At low speeds, the weight on spacing and trajectory tracking dominates to preserve cohesion and safety when hydrodynamic interactions are weak. At higher Froude numbers, the energy term gains importance so that the controller can exploit beneficial wake and pressure effects while respecting safety constraints.
4. The framework is evaluated on a three-vessel fleet sailing segments in platooning, triangular and echelon formations, as well as a free-formation configuration. Comparative simulations quantify how energy savings, tracking performance and safety margins trade off across formations and operating regimes, and illustrate the computational scalability of the proposed architecture for small fleets.

The choice for a hierarchical configuration-tracking structure reflects a compromise between model fidelity and online tractability. Centralized nonlinear MPC with full hydrodynamic coupling would in principle capture all interactions, but quickly becomes computationally prohibitive and hard to tune for larger fleets. Potential-field or purely kinematic approaches are lighter to implement, yet they typically lack a direct link to physically based resistance models and thus offer limited insight into energy savings. In contrast, the proposed architecture uses a reduced-order, Kelvin-wake-based resistance model in a small-scale nonlinear program at the supervisory level, while the tracking layer remains a standard, constraint-handling MPC. This yields an energy-aware controller that retains physical interpretability and remains implementable for small to medium-sized formations.

1.4. Outline

The remainder of this paper is organized as follows. Section 2 introduces the system dynamics of ASVs, the longitudinal and lateral interference force formulations, and the energy consumption model. Section 3 presents a hierarchical control framework, where the upper layer optimizes formation geometry for energy efficiency, and the lower layer applies MPC for trajectory tracking. In Section 4, sets up simulation scenarios and analyzes energy and tracking performance across formations. Section 5 concludes with a summary and suggests directions for future research.

2. System description

2.1. ASV kinematic and dynamic modeling

The formation system consists of multi autonomous surface vessel(ASV). The plane motion of a vessel can be described by the 3-DoF (degrees of freedom) kinematics and kinetics model. The model of the ASV_i is described based on Fossen (2011):

$$\begin{cases} \dot{\eta}_i = R_i(\psi_i)\nu_i \\ M_i\dot{\nu}_i = -C_i(\nu_i)\nu_i - D_i(\nu_i)\nu_i + \tau_{is}(\nu_i,\eta_i) + \tau_i, \end{cases} \tag{1}$$

where $\eta_i = \begin{bmatrix} x_i & y_i & \psi_i \end{bmatrix}^T$ is the vector denoting the ship position (x_i, y_i) and heading ψ_i with coordinates in the earth fixed frame; $\nu_i = \begin{bmatrix} u_i & v_i & r_i \end{bmatrix}^T$ is the vector denoting the ship velocities in the body fixed frame containing the velocity of surge u_i, sway v_i, and yaw r_i; The control input vector is $\tau_i = \begin{bmatrix} \tau_{iu} & \tau_{iv} & \tau_{ir} \end{bmatrix}^T \in \mathbb{R}^3$. The terms $M_i \in \mathbb{R}^{3\times3}$, $C_i \in \mathbb{R}^{3\times3}$, and $D_i \in \mathbb{R}^{3\times3}$ are the mass (inertia), Coriolis-Centripetal, and Damping matrix, respectively. Full details of the hydrodynamic coefficients can be found in Fossen (2011) The matrix $\tau_{is} = \begin{bmatrix} \tau_{isx}, \tau_{isy}, \tau_{isr} \end{bmatrix}^T \in \mathbb{R}^{3\times3}$ represents the ship to ship interaction forces and moments. The matrix $R_i(\psi_i) \in \mathbb{R}^{3\times3}$ denotes a rotation matrix, and is given below:

$$R_i(\psi_i) = \begin{bmatrix} \cos(\psi_i) & -\sin(\psi_i) & 0 \\ \sin(\psi_i) & \cos(\psi_i) & 0 \\ 0 & 0 & 1 \end{bmatrix}. \tag{2}$$

2.2. Formation geometric configuration

In this study, we focus on a three vessels formation system as the baseline configuration. This choice is motivated by several considerations. First, a meaningful formation system typically comprises at least three vessels, which enables the study of spatial coordination and interaction patterns beyond simple pairwise behaviors. Second, the geometric diversity of three vessels arrangements improves the generality of the results, allowing insights to be extended to larger fleets. Third, a symmetric three vessels configuration provides balanced lateral forces and yaw moments, contributing to greater formation stability. Compared to two vessel systems, three vessel formations exhibit greater potential for total resistance reduction and energy consumption optimization (He et al., 2022a).

A variety of formation geometries have been proposed in the literature, including platooning (Liu et al., 2017; Liang et al., 2021), parallel (Almeida et al., 2010), triangular (Liu and Bucknall, 2015; Peng et al., 2017), V shaped (Lv et al., 2022; Riahifard et al., 2019), echelon (Dong et al., 2022b) and grid based (Luo et al., 2024) configurations. Each structure offers trade offs in terms of hydrodynamic benefit, formation coverage, communication topology, and control complexity.

For instance, platooning formations maximize longitudinal wake-riding benefits and are relatively easy to coordinate, but they provide limited lateral coverage and can be vulnerable to traffic conflicts in bends and crossings. Triangular layouts offer wider footprints and improved observability for the leader, at the cost of more complex communication patterns and potentially stronger lateral interactions near the apex vessel. Echelon formations strike a compromise, enabling partial wake-riding along oblique tracks while preserving some lateral coverage, but they require careful tuning of both longitudinal and transverse gaps to avoid excessive sway and yaw loads. These trade-offs are consistent with observations from recent formation-control and hydrodynamic studies on multi-vessel systems (Zhao et al., 2025; He et al., 2022a; Dong et al., 2022b).

However, not all formations are suited for energy efficient operation. Specifically, some layouts, such as parallel, grid, or circular formations, tend to lack effective wake utilization and may introduce additional hydrodynamic disturbances such as lateral suction or yaw moment imbalance. As a result, they offer limited potential for propulsion power reduction.

Given that this study focuses on hydrodynamics aware energy optimization, we limit our attention to three representative formation geometries with promising energy saving characteristics: platooning, triangular, and echelon formations as shown in Fig. 1. These layouts not only enable better exploitation of wake effects but also offer distinct spatial arrangements for analyzing formation control under nonlinear interaction forces.

In the platooning formation (Fig. 1a), vessels are aligned along a longitudinal axis, with each follower maintaining the distance S_L from its predecessor. This configuration is known for its strong wake utilization effect, as downstream vessels benefit from reduced flow resistance by sailing within the wake field of the leading ship. Properly optimized spacing can reduce both frictional drag and wave making resistance, thereby enhancing fuel efficiency. However, platooning also presents challenges:

- **Wake stability:** When the spacing between vessels is excessively narrow, turbulent wake flows can destabilize the following vessel.

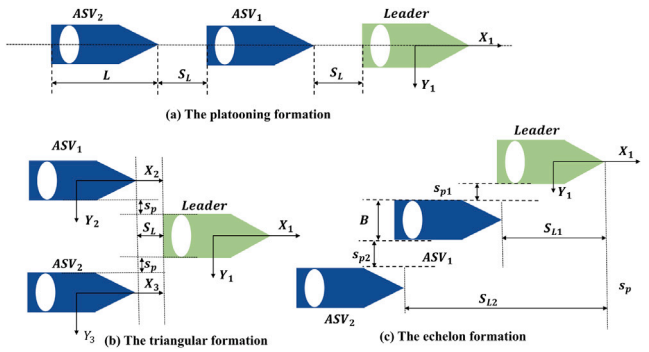

Fig. 1. The geometric configuration of formation.

- **Path adaptability:** Maintaining precise trajectory tracking is more critical compared to other formations, as minor deviations can lead to ineffective wake utilization.

In the triangular formation (Fig. 1b), the follower vessels are symmetrically arranged behind the leader, forming a staggered triangle. This layout strikes a balance between wake exploitation and lateral stability, making it a compromise between platooning and parallel formations. The triangular formation offers several advantages:

- **Distributed wake utilization:** Unlike platooning formations, where wake utilization is concentrated on a single vessel, the triangular configuration distributes the benefits across both follower vessels.
- **Improved hydrodynamic balance:** The offset arrangement reduces the risk of lateral suction and pressure imbalance, common in tightly spaced side by side formations.
- **Yaw moment suppression:** The symmetric structure minimizes yaw disturbances and enhances formation cohesion.

In the echelon formation (Fig. 1c), vessels are placed diagonally behind the leader, typically on the same side, forming a step like structure. This configuration allows partial wake usage for one follower while maintaining a relatively open lateral topology. This layout enables the trailing ships to intersect the wake region at an oblique angle, allowing them to avoid the turbulent wake core while still benefiting from reduced resistance due to favorable flow conditions. Its key features include:

- **Enhanced wake exploitation:** By entering the wake zone diagonally, the trailing vessel can harness the low pressure region without being subjected to high turbulence intensity.
- **Low trajectory overlap:** The formation minimizes path redundancy, enabling flexible motion planning and collision avoidance.

In summary, platooning, triangular, and echelon formations are selected in this study due to their demonstrated potential for hydrodynamic cooperation and energy savings. Each configuration offers distinct advantages in wake utilization, flow stability, and control feasibility. To quantify and compare their energy performance under realistic conditions, the next section develops a resistance based energy consumption model that incorporates ship to ship interaction effects.

2.3. Energy consumption modeling

Optimizing the energy consumption of multi vessel formations requires establishing a model for the overall energy consumption of the formation. The primary sources of energy loss during vessel navigation come from resistance, including frictional resistance, pressure resistance, wave making resistance, and ship to ship interaction forces. This section will develop an energy consumption model that incorporates these key factors and provides corresponding empirical formulas for use in the optimization of formation control.

The power demand of a vessel propulsion system can be expressed as (Molland et al., 2017):

$$P_T = \frac{R_T \times U}{\eta}, \tag{3}$$

where P_T denotes the total propulsive power, R_T represents the total resistance, and U is the vessel speed. The propulsive efficiency η typically ranges between $0.6 - 0.8$.

The total surge load on each vessel is written as the sum of calm-water resistance and additional interaction resistance,

$$R_{T,i} = R_{C,i} + F_{I,i}, \tag{4}$$

where $R_{C,i}$ denotes the calm-water resistance of vessel i sailing alone, and $F_{I,i}$ collects the change in resistance due to ship-to-ship interaction in formation. The corresponding surge component is included in the load vector τ_{is} in (1). Sway and yaw interaction loads are treated in a similar way and are mainly used to assess stability and safety margins in the simulations.

2.3.1. Calm-water resistance model

For a single vessel, the calm-water resistance is expressed in non-dimensional form as:

$$R_{C,i} = \frac{1}{2}\rho U_i^2 S C_{T,C}(Fr_i), \tag{5}$$

where ρ is the water density, U_i is the speed through water, S is the wetted surface area, $Fr_i = U_i/\sqrt{gL}$ is the Froude number based on the waterline length L, and $C_{T,C}(Fr)$ is the calm–water total resistance coefficient. In this work:

$$C_{T,C}(Fr) = C_F(Re) + C_P + C_W(Fr), \tag{6}$$

where C_F follows the ITTC–1957 line, C_P is a constant form factor and $C_W(Fr)$ represents the wave-making contribution obtained from a standard resistance curve for the chosen hull form (International Towing Tank Conference, 1957; Molland et al., 2017).

2.3.2. Additional interaction resistance model

In multi vessel formations, wave interference induced by the leading vessel produces additional hydrodynamic effects on following vessels. The key factors affecting this additional interaction forces include formation spacing, which include longitudinal distance S_L and lateral distance S_p, and vessel speed U, both of which affect the hydrodynamic interactions among ships. These interactions yield wake utilization benefits, lateral suction forces, and pressure differentials, all of which collectively determine the total resistance encountered by each vessel. Although there are other influencing factors, like the environmental disturbances such as wind, wave and current, they are neglected in this study.

The distance between vessels in a formation profoundly influences the magnitude of hydrodynamic interactions. Depending on the configuration, inter vessel spacing can result in either a reduction in resistance—via effective wake utilization, or an increase in resistance due to undesirable interference effects. Moreover, vessel speed plays a critical role in determining both the nature and magnitude of ship to ship interaction forces. To accurately evaluate energy consumption and optimize control, it is essential to formulate a theoretical model that reflects the wave induced resistance variation at each follower vessel location.

A surface vessel sailing at constant speed generates a V shaped Kelvin wake characterized by transverse and diverging waves. Under linear potential flow theory, and assuming small amplitude (small disturbance) waves (Newman, 2018), the free surface elevation generated by a single vessel can be approximated by:

$$\eta_{ij}(x_{ij}, y_{ij}) = A\cos(kx_{ij} + k_y y_{ij}) \tag{7}$$

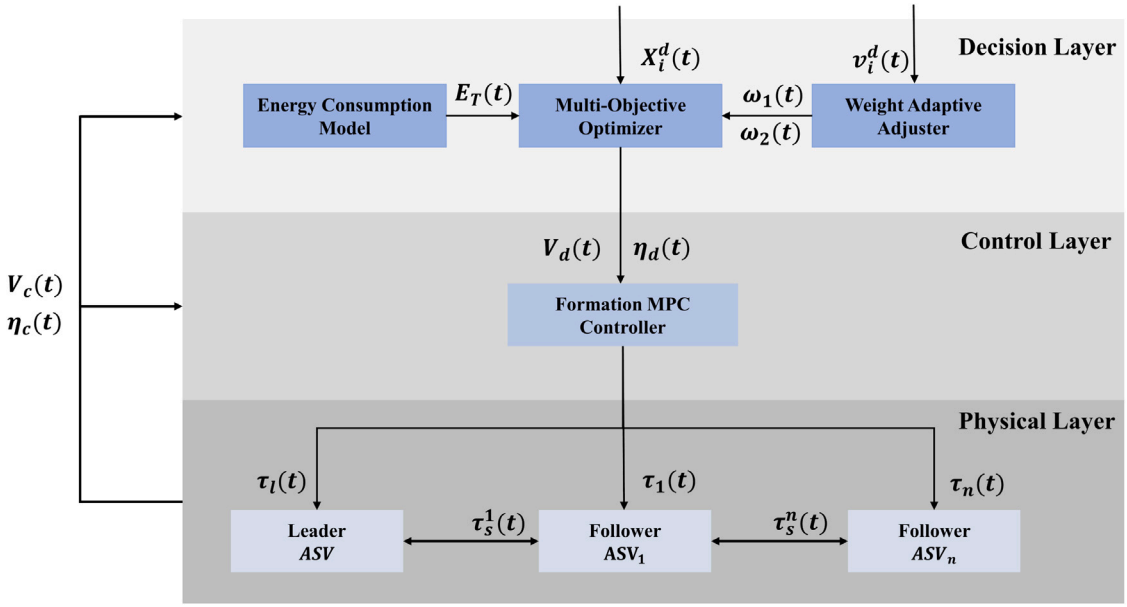

Fig. 2. Formation control structure.

where η_{ij} is the free surface elevation generated by the ASV_j at the location of ASV_i. $x_{ij} = |x_i - x_j|$ and $y_{ij} = |y_i - y_j|$ represent the longitudinal and lateral spacing between ASV_i and ASV_j. A is the wave amplitude, $k = 2\pi/\lambda$ is the longitudinal wave number, $k_y = k\tan\theta_K$ is the lateral wave number associated with the Kelvin angle $\theta_K \approx 19.47°$, and λ is the dominant wavelength.

For each follower i, only the most influential upstream vessels are considered. In this work, we assume that at most two upstream neighbors contribute significantly to the wave field at i, namely the leader and, when present, the closest preceding follower on the same side of the formation.

Let $\mathcal{N}_i$ denote the set of upstream neighbors of vessel i. To keep the interaction model simple and focused on dominant effects, $\mathcal{N}_i$ is restricted to at most two vessels: the leader and, if applicable, the closest follower directly ahead of i in the same lane. The free-surface elevation at follower i is then approximated as:

$$\eta_i = \sum_{j\in\mathcal{N}_i} \eta_{ij}(x_{ij}, y_{ij}), \tag{8}$$

where η_{ij} is the Kelvin-wave contribution generated by vessel j at the position of vessel i.

According to linear wave theory (Dean and Dalrymple, 1991), the pressure perturbation near the free surface is approximately proportional to the local slope of the wave elevation, represented by the spatial gradient of η. This relationship can be simplified as:

$$\Delta p \propto \nabla\eta, \tag{9}$$

where $\nabla\eta$ denotes the surface gradient, reflecting the local wave induced tilt. This approximation is widely used in small disturbance hydrodynamic models to relate wave shape to pressure field variation.

The additional resistance acting on the ASV_i due to ship to ship interaction can be assumed proportional to the square of the local slope, representing the magnitude of wave impact regardless of its direction:

$$F_{I_i} \propto \left(\frac{\partial\eta_i}{\partial x}\right)^2. \tag{10}$$

However, this formulation cannot distinguish between thrust aiding and thrust resisting effects, since it is always non negative.

To account for the thrust and resistance distinction: Riding in a wave trough induces a propulsive effect (drag reduction). Riding on a wave crest induces resistance (drag increase). Thus, the model is refined to incorporate curvature:

$$F_{I_i} \propto \eta_i \times \frac{\partial^2\eta_i}{\partial x^2}. \tag{11}$$

To further refine this expression and account for slope directionality, which affects wave loading asymmetry, we introduce a slope sign term:

$$F_{I_i}(x) = K \times \eta_i \times \frac{\partial^2\eta_i}{\partial x^2} \times \mathrm{sign}\left(\frac{\partial\eta_i}{\partial x}\right), \tag{12}$$

where F_{I_i} denotes the additional ship to ship interaction forces of ASV_i, K is a proportionality constant, $\mathrm{sign}(\cdot)$ indicates the slope direction.

Consequently, the energy consumption model for formation comprising three ASVs can be expressed as follows:

$$E_T = \sum_{i=1}^{3}\left(R_{C,i} \times V_i\right) + \sum_{i=2}^{3}\left(F_{I,i} \times V_i\right). \tag{13}$$

where the first summation captures the calm-water contributions and the second summation adds the interaction-induced resistance of the followers.

Assumptions and validity. The interaction model is a reduced-order approximation based on linear Kelvin-wave theory. The flow is assumed inviscid and irrotational, the free-surface disturbance is small, and the dominant wave component of each vessel is represented by a single harmonic with fixed Kelvin angle and wavelength. Superposition is applied, but for each follower only the leader and at most one additional upstream follower on the same side are taken into account, since more distant vessels have a much weaker influence in the close-spacing regimes considered here. The model is intended to capture qualitative trends, not exact loads, and is used to guide spacing and layout optimization in the hierarchical MPC framework rather than to replace detailed hydrodynamic analysis.

3. Formation control framework

Building on the modeling in Section 2, this section presents a hierarchical formation-control framework that integrates the Kelvin-wave-based interaction model into an online optimization and tracking scheme. The architecture, sketched in Fig. 2, the framework is composed of three layers: the decision layer, the control layer, and the physical layer.

Decision layer: At this level, the current sailing speed $V_c(t)$ and configuration state $\eta_c(t)$ are the input into an *Energy Consumption Model* to evaluate the total energy $E_T(t)$. *Weight Adaptive Adjuster* determines the trade off between energy efficiency and formation accuracy through dynamic weight coefficients $\omega_1(t)$ and $\omega_2(t)$, based on speed sensitive mechanisms (e.g., Froude number driven sigmoid functions). These are passed to a *Multi Objective Optimizer*, and also the initial state of formation X_i^d. The optimizer outputs the optimal desired speed $V_d(t)$ and spatial configuration $\eta_d(t)$, which are transmitted to the lower layer.

Control layer: The *Formation MPC Controller* receives $V_d(t)$ and $\eta_d(t)$ as reference targets and generates real time control commands $\tau_i(t)$ for each ASV, taking into account system dynamics, control constraints, and predicted ship to ship interaction effects.

Physical layer: This layer represents the actual vessel fleet, consisting of a leader ASV and multiple follower ASVs. Each vessel executes the thrust and steering commands $\tau_i(t)$ computed by the MPC controller. Additionally, the current vessel velocities $V_c(t)$ and states $\eta_c(t)$ are continuously monitored and sent back to both the lower and upper layers.

This section presents a hierarchical control architecture composed of a top level formation supervisory controller and bottom level local MPC controllers. This two layer design allows for global energy efficient decision making while ensuring robust real time execution for each vessel. As shown in Fig. 2, the top level controller receives as input a set of desired formation configuration parameters, The supervisory controller solves an optimization problem to compute the optimal spacing and trajectories that minimize overall energy consumption while maintaining formation geometry and tracking performance. These optimal reference values are transmitted to each vessel's local MPC controller.

At the lower level, each MPC controller computes thrust and steering commands that guide the vessel to its assigned position while considering local dynamics, control constraints, and interaction effects. This separation of roles ensures global coordination and local adaptability, supporting the formation's energy efficiency and safety goals.

3.1. Decision layer

3.1.1. Energy consumption model

The energy consumption model estimates the total energy expenditure of the formation for a given configuration. Its inputs are the relative positions and velocities of all vessels, and it evaluates the instantaneous total energy $E_T(t)$ according to (13).

At each time step, the value of $E_T(t)$ is passed to the supervisory optimizer, which uses it with formation keeping terms to compute the desired speed and spatial configuration that minimize total energy while maintaining the prescribed formation geometry and control objectives.

3.1.2. Optimizer

To enable adaptive trade offs between energy efficiency and formation accuracy, a multi objective optimization module is employed to determine the optimal spatial configuration of the vessel formation. The optimizer operates at each time step using a cost function that jointly considers energy consumption and deviation from the desired geometric layout.

To ensure numerical consistency between objectives, both terms are normalized by reference values. In particular, the energy term is normalized using a baseline energy E_{ref}, defined as the total propulsion power required by all vessels operating independently without any ship to ship interactions. This baseline serves as a physically meaningful upper bound for evaluating formation induced energy savings. The optimization problem is formulated as:

$$\begin{aligned} \min_{\{d_{ij}\}} \quad & \sum_{i=1}^{3} \left[\omega_1(t) \frac{E_i(d_{ij})}{E_{\text{ref}}} + \omega_2(t) \frac{\left\| X_i(d_{ij}) - X_i^{\text{d}} \right\|_2^2}{D_{\text{ref}}^2} \right] \\ \text{s.t.} \quad & d_{ij}^{\min} \le d_{ij} \le d_{ij}^{\max}, \\ & d_{ij} \in \mathcal{D}_{\text{geom}}, \qquad \forall (i,j), \end{aligned} \tag{14}$$

where d_{ij} denotes the relative distance between ASV_i and ASV_j. $X_i(d_{ij})$ and X_i^d denote the actual and desired positions of ASV_i. $E_{\text{ref}} = \sum_{i=1}^{N} R_i^{\text{free}} \cdot V_i$ is the total propulsion energy of all vessels in non interacting navigation; D_{ref} is a reference distance scale, the maximum allowable deviation from the desired position. ω_1 and ω_2 are the adaptive weights defined in the next subsection, whose values are related to the current desired speed. $\mathcal{D}_{\text{geom}}$ collects simple geometric constraints such as minimum separation. The output is a set of optimal desired distances d_{ij}^*, which are sent to each vessel's MPC controller as reference targets.

For clarity and reproducibility, Table 1 summarizes the main elements of the optimization problem (14).

Table 1
Summary of supervisory optimization problem.

Symbol	Role	Domain/value
d_{ij}	Inter-vessel spacing (longitudinal/lateral)	$[d_{ij}^{\min}, d_{ij}^{\max}]$
E_i	Instantaneous energy of vessel i	$\mathbb{R}_{\ge 0}$
X_i^d	Reference position of vessel i	$\mathbb{R}^2$
ω_1, ω_2	Weights for energy/formation error	$[0,1]$, $\omega_1 + \omega_2 = 1$
E_{ref}	Baseline energy (solo sailing)	Given constant
D_{ref}	Reference position deviation	Given constant
$\mathcal{D}_{\text{geom}}$	Geometric and safety constraints	Min. gap, layout bounds

In the current implementation, (14) is a small-scale nonlinear programmer in the spacing variables. It is solved at each decision step using a sequential quadratic programming method (MATLAB `fmincon`, interior-point option), with gradients obtained by finite differences. Because the optimization is static and low-dimensional for the three-vessel case, convergence is typically achieved in a few iterations, and the computational effort remains well below the MPC sampling time. The structure of (14) also scales favorably with the number of vessels: the number of decision variables grows with the number of spacings, while the evaluation of $E_i(d_{ij})$ relies on pairwise interaction terms. For larger formations, symmetry or parametric spacing patterns can be used to keep the problem size manageable.

3.1.3. Weight adaptive adjuster

To enable context aware optimization under varying operational conditions, this module dynamically adjusts the control weights ω_1 and ω_2 in the multi objective cost function. The primary basis for adjustment is the desired sailing speed V_d, which reflects strategic navigation goals such as cruising, maneuvering, or port operations.

The rationale for this design stems from the strong correlation between vessel speed and hydrodynamic behavior in formation sailing. At higher speeds, wave making resistance becomes the dominant component of total drag. In such regimes, inter vessel wake interactions offer significant energy saving potential by allowing following vessels to benefit from reduced resistance. To capitalize on this effect, the controller prioritizes energy minimization by assigning a higher weight to the energy term ω_1, while reducing emphasis on trajectory accuracy.

Conversely, at lower speeds – such as during docking, channel navigation, or obstacle avoidance – the influence of wave making resistance is significantly diminished. Under these conditions, maintaining accurate geometric alignment and safe maneuverability is more

Algorithm 1 Higher Layer Supervisory Control

Require: Current formation configuration $V_c(t)$ and $\eta_c(t)$, desired formation shape X_i^d, desired speed v_d.

Ensure: Optimal inter vessel spacing $d_{ij}^*(t)$, Reference positions $\eta_d^i(t)$, Reference velocities $V_d^i(t)$.

1: **Step 1: Energy Estimation** Compute total energy consumption $E_T(t)$ under current formation configuration using the energy model according to (13).

2: **Step 2: Weight Adjustment** Compute the adaptive weights $\omega_1(t), \omega_2(t)$ using either speed based or Froude number based strategy ((15) or (16)).

3: **Step 3: Multi objective Optimization** Solve the optimization problem according to the cost function (14), subject to hydrodynamic constraints and geometric limits.

4: **Step 4: Reference Propagation** Send the optimal reference position $\eta_d^i(t)$ and velocity $V_d^i(t)$ for each vessel i to the local MPC controller.

critical. Therefore, the weight ω_2 associated with formation tracking is increased accordingly.

The Froude number is commonly used to determine the hydrodynamic regime corresponding to a vessel's speed. When $F_r < 0.2$, the vessel is considered to be in a low speed regime; when $0.2 \leq F_r \leq 0.4$, it is in a medium speed regime; and when $F_r > 0.4$, it is regarded as operating at high speed. To adapt the control weights to the vessel's hydrodynamic regime, the weighting function is formulated as a sigmoid function of the Froude number F_r. This allows the system to prioritize tracking accuracy at low speeds and energy efficiency at higher speeds. The weighting function is defined as:

$$\omega_1(t) = \frac{1}{1 + e^{-\lambda(F_r(t) - F_{r0})}}, \tag{15}$$

$$\omega_2(t) = 1 - \omega_1(t), \tag{16}$$

where $F_r(t) = \frac{V_d(t)}{\sqrt{gL}}$, F_{r0} is the critical Froude number (typically 0.2), and λ controls the transition steepness. This formulation ensures smooth and responsive weighting adjustment aligned with hydrodynamic energy saving characteristics.

In summary, the algorithm flow in the higher layer control is summarized in Algorithm 1.

3.2. Control layer

The local controller for each vessel is implemented within a Model Predictive Control (MPC) framework, which enables real time trajectory tracking, inter vessel coordination, and constraint handling. At every control step, each vessel receives its reference position $\eta_d^i(t)$ and reference velocity $v_d^i(t)$ from the decision layer. Based on these references, the MPC computes the optimal control input $\tau_i(t)$ that minimizes control effort while ensuring accurate trajectory tracking and compliance with operational constraints.

In addition to conventional vessel dynamics and input constraints, the local controller also considers hydrodynamic interaction forces that arise due to the proximity of neighboring vessels. These interaction forces – primarily induced by wake effects and flow interference – can alter the effective resistance experienced by each vessel.

To incorporate the hydrodynamic interaction force F_I derived from Section 2 into the control inputs of the local MPC, it is necessary to transform this scalar force – defined along the line of action between vessels – into the three degrees of freedom (DOF) generalized force vector in the vessel's body fixed coordinate frame.

The transformation is achieved using a directional mapping matrix $\mathbf{J}(\psi_{ij})$, which projects the interaction force into surge, sway, and yaw components based on the relative bearing angle ψ_{ij} between the interacting ASV_i and ASV_j:

$$\tau_{is}(t) = \begin{bmatrix} \tau_{isx}(t) \\ \tau_{isy}(t) \\ \tau_{isr}(t) \end{bmatrix} = \mathbf{J}(\psi_{ij}) \cdot F_I, i(t), \tag{17}$$

where $\mathbf{J}(\psi_{ij})$ is the rotation matrix that transforms coordinated based on the direction angle ψ_{ij} of the neighboring vessel. The matrix is given below:

$$\mathbf{J}(\psi_{ij}) = \begin{bmatrix} \cos(\psi_{ij}) \\ \sin(\psi_{ij}) \\ l_i \sin(\psi_{ij}) \end{bmatrix} \tag{18}$$

where l_i being the transverse distance from the center of gravity to the point of action. This formulation ensures that the scalar hydrodynamic interaction force F_I is correctly incorporated into the multi DOF dynamics of each vessel.

Define a new system state $\boldsymbol{x}^i(k) = \begin{bmatrix} \boldsymbol{\eta}^i(k) \\ \boldsymbol{\nu}^i(k) \end{bmatrix}$. At each sampling instant, the MPC controller solves the following optimization problem over a prediction horizon N_p and control horizon N_c:

$$\begin{aligned} \min_{\Delta\boldsymbol{\tau}^i(k)} \; & \sum_{k=0}^{N_p} \left\| \boldsymbol{x}^i(k) - \boldsymbol{x}_d^i(k) \right\|_{\mathbf{Q_i}}^2 + \sum_{k=0}^{N_c} \left\| \Delta\boldsymbol{\tau}^i(k) \right\|_{\mathbf{R_i}}^2 \\ \text{s.t.} \quad & \boldsymbol{x}^i(k+1) = \mathbf{f}(\boldsymbol{x}^i(k), \boldsymbol{\tau}^i(k)), \\ & \boldsymbol{\tau}^i(k) = \boldsymbol{\tau}^i(k-1) + \Delta\boldsymbol{\tau}^i(k), \\ & \boldsymbol{\nu}_{\min} \leq \boldsymbol{\nu}^i(k) \leq \boldsymbol{\nu}_{\max}, \\ & \boldsymbol{\tau}_{\min} \leq \boldsymbol{\tau}^i(k) \leq \boldsymbol{\tau}_{\max}, \\ & \Delta\boldsymbol{\tau}_{\min} \leq \Delta\boldsymbol{\tau}^i(k) \leq \Delta\boldsymbol{\tau}_{\max}. \end{aligned} \tag{19}$$

where $\boldsymbol{\eta}^i(k)$ denotes the predicted state of vessel i at time step k, and $\boldsymbol{\eta}_d^i(k)$ represents the desired reference trajectory assigned to vessel i. $\boldsymbol{\nu}^i(k)$ denotes the predicted velocity of vessel i at time step k, and $\boldsymbol{\nu}_d^i(k)$ represents the desired velocity assigned to vessel i. The term $\Delta\boldsymbol{\tau}^i(k)$ denotes the control increment, which penalizes rapid changes in thrust or rudder input to ensure smooth actuation. $\mathbf{Q_i}$ and $\mathbf{R_i}$ are the weighting matrices that balance the importance between trajectory tracking accuracy and control effort, respectively.

The main process steps of the local control are summarized in Algorithm 2.

Algorithm 2 Low Layer Local Control

Require: Predicted hydrodynamic interaction $\tau_{is}(t)$, reference trajectory $\eta_d^i(t)$, $V_d^i(t)$ from the supervisor controller, current vessel state $x_i(t)$.

Ensure: Optimal control input $\tau^i(t)$ for each vessel at current time step according to (17)–(18).

1: **Step 1:** Construct the augmented system state to the $x^i(k)$.

2: **Step 2:** Compute thruster forces and moments $\tau_i(t)$ according to the cost function, system dynamics and constrains (19).

3: **Step 3:** Repeat from Step 1 at next time with updated states.

4. Simulation and experiments

To evaluate the effectiveness of the proposed control framework, a series of experiments are conducted, followed by a detailed discussion and analysis of the results. The test cases focus on three representative formation configurations – platooning, triangular, and echelon – allowing a comparative assessment of energy efficiency and control performance under typical spatial layouts.

The experiments employ the "TitoNeri" model developed by the Researchlab Autonomous Shipping (RAS) at Delft University of Technology. The hydrodynamic parameters of the model are documented

in Haseltalab and Negenborn (2019). To capture high speed operational behavior, the thrust input limits are scaled to enable a maximum vessel speed of approximately 1.5 m/s. This setup ensures a representative evaluation of the proposed control strategy under dynamic maneuvering conditions.

Two operational regimes are considered. At low speeds, the control objective emphasizes maintaining high formation keeping accuracy and precise trajectory tracking, which are essential for navigational safety and structural cohesion within the fleet. In this regime, hydrodynamic interactions are relatively weak, and the control system prioritizes stability and robustness. At higher speeds, hydrodynamic effects – such as wake interactions and lateral suction – become more pronounced and significantly affect energy consumption. Under these conditions, the control focus shifts toward minimizing total fleet energy usage by exploiting these interactions through optimized formation configurations.

To test the behavior under varying speed conditions, a piecewise constant reference speed profile was designed to simulate gradual acceleration and deceleration. The profile spans a total of $N_{\text{steps}} = 360$ discrete time steps, divided into uniform step intervals of $\Delta n = 30$ steps each.

The reference speeds were defined to increase linearly from a minimum value $U_{\min} = 0.1\,\text{m/s}$ to a maximum value $U_{\max} = 1.5\,\text{m/s}$, and then decrease back to $U_{\min}$. The resulting stair shaped speed levels are stored in the vector $U_{\text{levels}} = [U_1, U_2, \ldots, U_{n_{\text{intervals}}}]$, where:

$$n_{\text{intervals}} = \left\lceil \frac{N_{\text{steps}}}{\Delta n} \right\rceil,$$

For any normalized simulation time $t \in [0, 1]$, the corresponding reference speed is defined by:

$$U_{\text{ref}}(t) = U_{\text{levels}}(k), \quad \text{where} \quad k = \left\lceil \frac{t \cdot N_{\text{steps}}}{\Delta n} \right\rceil \tag{20}$$

4.1. Experiment I: Platooning formation

To evaluate the performance of energy efficient platooning formations under variable speed navigation, we conducted a simulation experiment where three ASVs were arranged in a linear formation. The initial configuration was set with a longitudinal separation of 1 meter and zero lateral offset between adjacent vessels.

The core objective of this simulation is to investigate the impact of speed adaptive formation control based on a multi objective optimization framework. Specifically, the formation is expected to maintain trajectory tracking accuracy at low speeds while minimizing total energy consumption at higher speeds by adjusting the inter ship distances dynamically.

Additionally, to ensure that the vessels maintain a platooning formation throughout the simulation, an additional spatial constraint is imposed on the lateral spacing between ships. Specifically, the lateral distances S_{p1} and S_{p2} between the leading vessel and each follower are restricted as:

$$S_{p1},\ S_{p2} \leq 0.1\,\text{m} \tag{21}$$

Fig. 3 shows the trajectories of the leader and two followers during the platooning simulation under the variable-speed reference profile. The leader follows a straight trajectory along the X-axis, while the two followers adjust their positions according to the decisions of the upper layer. As speed increases, the longitudinal distances gradually grow, reflecting the controller's tendency to enlarge spacing at higher speeds in order to exploit favorable wake regions and reduce resistance. When the reference velocity decreases, the inter-ship distances smoothly return toward their initial configuration, indicating that formation cohesion and tracking accuracy are again prioritized at low speeds.

Fig. 4 illustrates the time evolution of surge velocity u, sway velocity v, and yaw rate r for the three vessels in platooning formation. It can be observed that all three vessels maintain consistent velocity profiles, reflecting the effectiveness of the control scheme in ensuring dynamic synchronization and coordination within the formation.

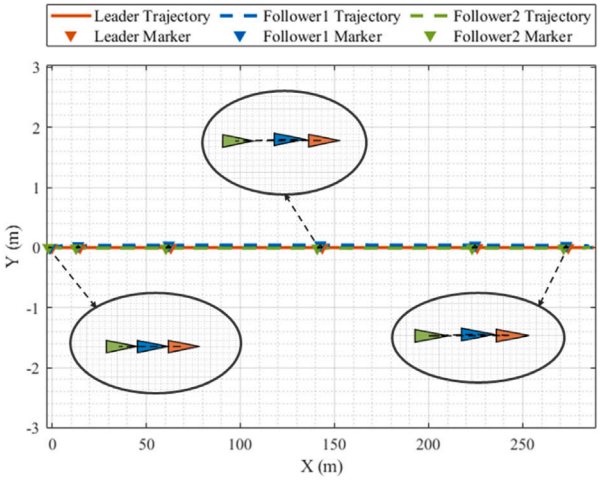

Fig. 3. The trajectories of three ASVs under platooning formation.

Fig. 5 illustrates the tracking performance of both longitudinal and lateral distances between the leader and each follower during the platooning formation maneuver. The black lines represent the desired reference distances, while the blue and green lines correspond to the actual longitudinal and lateral distances, respectively.

It can be observed that as the reference speed increases, the longitudinal distances between vessels gradually expand in accordance with the optimized spacing strategy. This behavior reflects the top layer controller's ability to adaptively adjust inter ship separation to minimize overall energy consumption at higher speeds. The lateral deviations remain minimal throughout most of the trajectory, confirming that the followers are able to maintain alignment behind the leader in a nearly ideal platooning configuration.

Once the speed begins to decrease, both the longitudinal and lateral distances return smoothly to their nominal values. This demonstrates the effectiveness of the formation control scheme in balancing energy saving objectives and formation accuracy across varying speed regimes.

To quantitatively evaluate the effectiveness of energy saving in the platooning formation, we compare the total energy consumption in the formation scenario with a non cooperative (solo navigation) baseline. The total energy consumption E_T in the formation is computed by summing the propulsion power of each ASV, including the effects of hydrodynamic interactions as Eq. (13).

For comparison, the baseline energy consumption E_T^{base} assumes each vessel sails independently without interaction forces:

$$E_T^{\text{base}} = \sum_{i=1}^{3} \left(R_{C,i} \cdot V_i \right) \tag{22}$$

The overall energy consumption percentage index $\%EC$ is then defined as:

$$\%EC = \frac{E_T - E_T^{\text{base}}}{E_T^{\text{base}}} \times 100 \tag{23}$$

A negative value of $\%EC$ indicates net energy savings due to formation effects, while a positive value reflects increased energy usage due to unfavorable interactions or poor coordination.

Fig. 6 presents the temporal evolution of the total energy consumption index %EC alongside the longitudinal and lateral tracking errors of both followers in the platooning formation.

As can be observed, the energy consumption index exhibits dynamic fluctuations as the formation transitions through different speed levels.

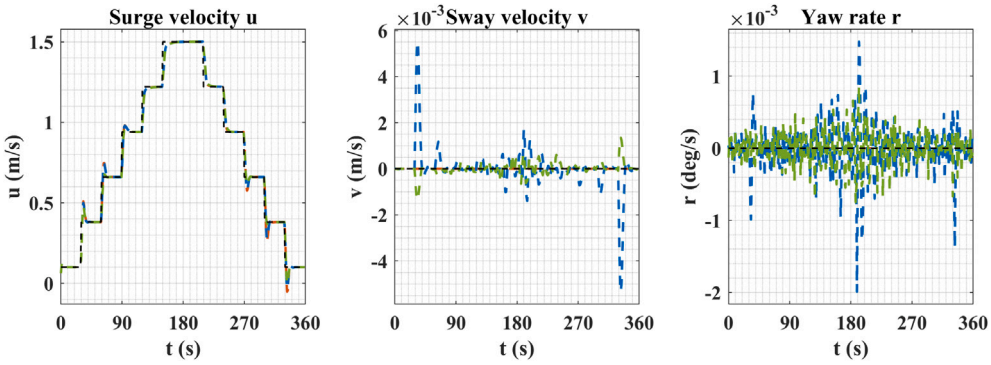

Fig. 4. Velocity response of the leader and followers in platooning formation. **Black**: reference velocity, **Orange**: leader, **Blue**: follower 1, **Green**: follower 2.

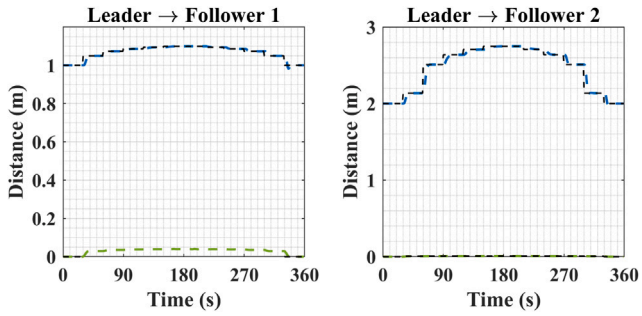

Fig. 5. Tracking performance of inter-ship distances in the platooning formation. **Black**: reference distance, **Blue**: actual longitudinal distance, **Green**: actual lateral distance.

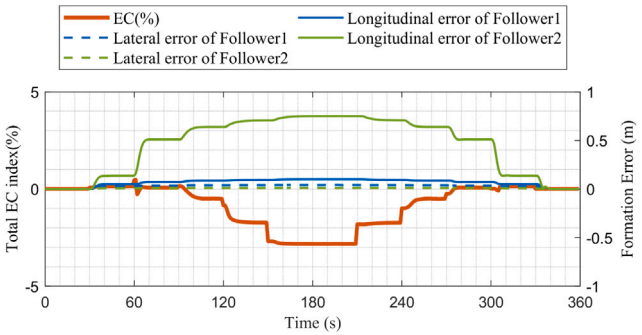

Fig. 6. Energy Consumption Index and Formation Tracking Errors Over Time.

During the mid to high speed phase (approximately $t = 120\,\text{s}$ to $t = 240\,\text{s}$), the %EC index drops below zero, indicating a net energy saving effect. This is attributed to the increased inter ship spacing, which allows the follower vessels to enter hydrodynamically favorable regions in the leader's wake and Kelvin wave field, effectively reducing wave resistance.

Meanwhile, the lateral and longitudinal errors of Follower 1 and Follower 2 remain within acceptable ranges. A slight increase in lateral deviation is observed during the energy saving phase, suggesting a trade off between maximizing energy efficiency and maintaining tight formation geometry.

Outside the energy saving region, especially at low speeds near the start and end of the simulation, the %EC index returns to near zero or positive values. This implies that the benefits from hydrodynamic interaction are limited or even negative under closely spaced, low speed conditions. In these cases, the controller prioritizes formation accuracy by reducing spacing, even at the cost of higher energy usage.

Overall, Experiment I confirms that the energy-aware formation controller can reduce propulsion energy in a platooning layout while keeping formation deviations and safety margins within acceptable limits.

4.2. Experiment II: Triangular formation

The triangular formation, similar with the platooning structure, is designed to exploit hydrodynamic interaction effects such as wake utilization and Kelvin wave overlap. Unlike the linear alignment of platooning formations, the triangular layout provides symmetric spacing of the follower vessels relative to the leader, enabling both enhanced flow exposure and formation stability.

In this scenario, the initial state of the formation is configured with a longitudinal spacing of 1.0 m and a lateral displacement of 0.5 m for the two follower vessels, symmetrically placed on either side of the leader.

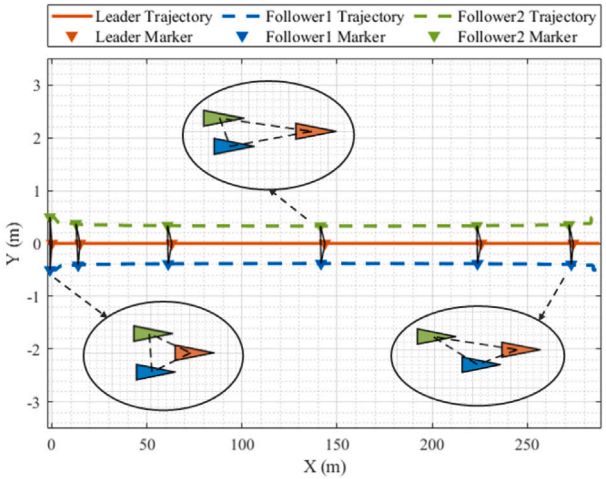

Fig. 7. The trajectories of three ASVs under triangular formation.

To maintain symmetry and safety, a constraint is enforced such that the sum of the lateral distances satisfies:

$$|S_{p1} + S_{p2}| < 0.1\,\text{m} \tag{24}$$

Fig. 7 shows the trajectories of the leader and followers. The leader sails steadily along the X-axis, while the followers adapt their positions according to the variable-speed reference. At higher speeds, the longitudinal distances increase to mitigate yaw disturbances and exploit wake effects; when the speed decreases, the formation gradually returns to the initial compact triangular structure.

The surge, sway, and yaw velocity curves show good tracking accuracy, and lateral/yaw fluctuations remain within safe bounds, validating the stability and control performance as shown in Fig. 8.

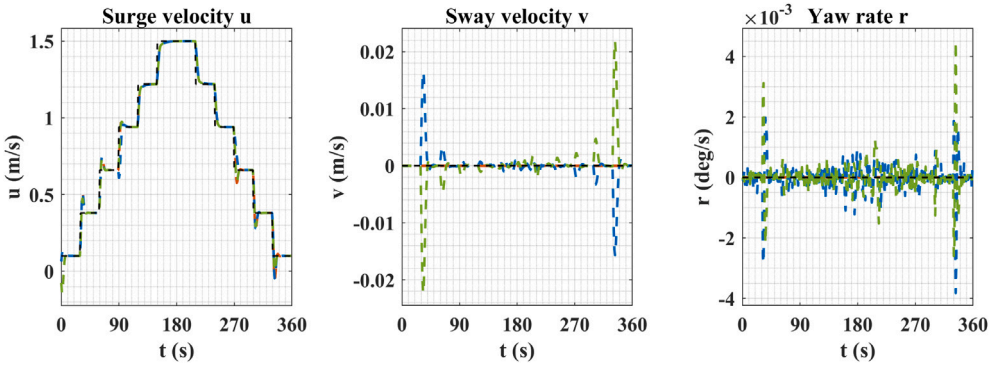

Fig. 8. Velocity response of the leader and followers in triangular formation. **Black**: reference velocity, **Orange**: leader, **Blue**: follower 1, **Green**: follower 2.

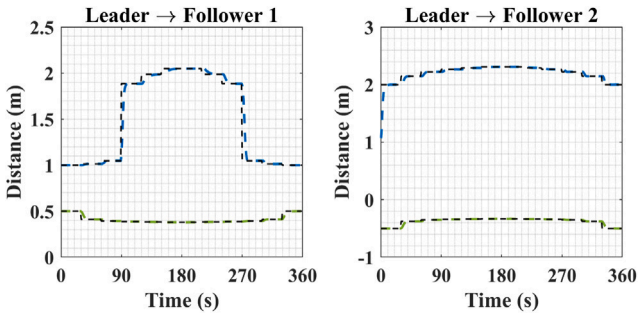

Fig. 9. Tracking performance of inter ship distances in the triangular formation. **Black**: reference distance, **Blue**: actual longitudinal distance, **Green**: actual lateral distance.

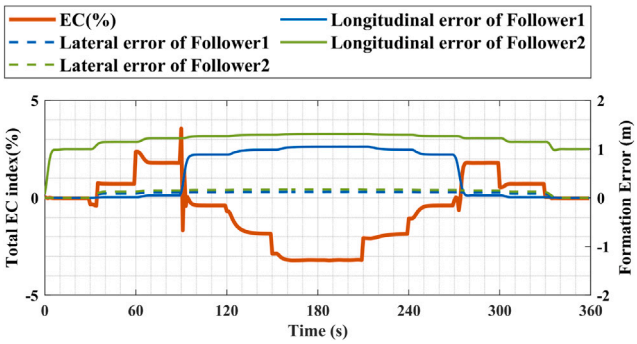

Fig. 10. Energy Consumption Index and Formation Tracking Errors Over Time.

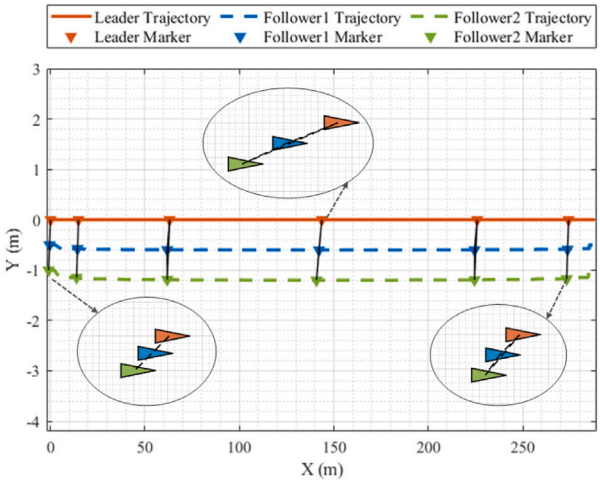

Fig. 11. The trajectories of three ASVs under echelon formation.

And we observe that the yaw rate in the triangular case remains lower and more stable than in the platooning configuration. This is because the symmetric triangular layout inherently reduces asymmetrical wake interference that might otherwise induce turning moments.

Fig. 9 shows the longitudinal and lateral distances between the leader and the followers. Similar to the platooning case, longitudinal distances expand in the medium-to-high-speed range and contract when speed decreases, but the lateral offsets remain symmetric.

In Fig. 10, both formations demonstrate energy savings (negative $\%EC$) at medium to high speeds. However, the triangular formation shows smoother transitions and slightly lower peak savings compared to platooning, due to its lateral constraints limiting optimal spacing flexibility.

In summary, the triangular formation strikes a balance between hydrodynamic energy saving benefits and spatial symmetry constraints. Compared to the platooning setup, it achieves comparable energy efficiency under high speed conditions while offering improved directional stability due to its symmetric wake alignment. These characteristics make triangular formations particularly attractive for coordinated operations requiring both efficiency and structural coherence.

4.3. Experiment III: Echelon formation

Compared with the previous two configurations, the echelon formation arranges both follower vessels on the same side of the leader in a diagonal alignment, enabling them to enter the leader's wake and Kelvin wave field at an oblique angle. This allows the followers to avoid the turbulent core while benefiting from favorable hydrodynamic interactions for drag reduction. This experiment evaluates the combined energy-tracking performance of the echelon structure under variable speed sailing.

The initial longitudinal spacings are set to $(S_{L,2}, S_{L,3}) = (0.5\,\mathrm{m}, 1.0\,\mathrm{m})$, and the lateral offsets to $(S_{P,2}, S_{P,3}) = (0.5\,\mathrm{m}, 1.0\,\mathrm{m})$, with all vessels placed on the same side to avoid track crossing. To maintain the echelon hierarchy and ensure safety, the following geometric constraints are imposed:

$$S_{P,3} \geq S_{P,2} + \varepsilon, \quad S_{L,3} \geq S_{L,2} + \varepsilon, \quad \varepsilon = 0.01. \tag{25}$$

Other weights and the speed profile were identical to Experiment I, with the top layer adaptively adjusting the energy or tracking weight according to the Froude number.

Fig. 11 shows three representative time instants. During the medium high speed phase, the formation spontaneously stretches into a stable echelon structure: the followers align along a diagonal "stair step" pattern relative to the leader, maintaining a clear longitudinal offset.

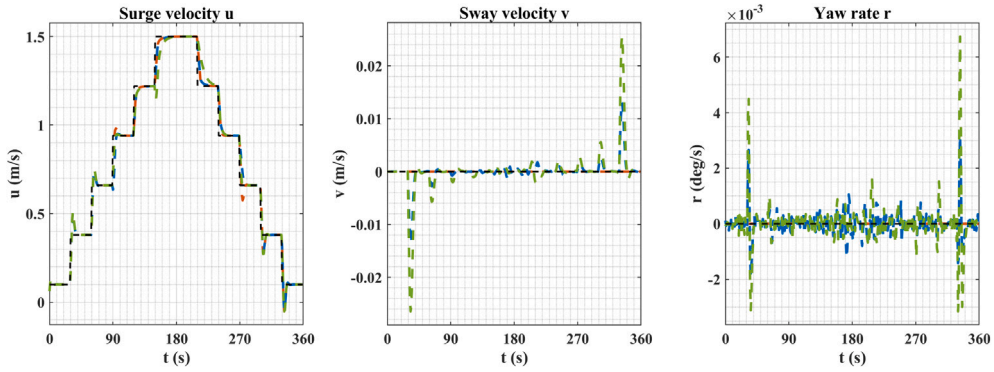

Fig. 12. Velocity response of the leader and followers in echelon formation. **Black**: reference trajectory, **Orange**: leader, **Blue**: follower 1, **Green**: follower 2.

The black arrows highlight the persistent relative positions within the leader's favorable wake sector. The enlarged circles further illustrate the smooth geometric transitions through acceleration, cruising, and deceleration phases, with the formation gradually contracting at low speeds while retaining the echelon layout.

Fig. 12 presents the u, v, r responses of all vessels. The longitudinal speed u closely follows the reference for all vessels. The lateral velocity v remains minimal, with only negligible perturbations at acceleration/deceleration transitions. The yaw rate r exhibits near zero mean oscillations with lower amplitudes than in the parallel case, indicating that the echelon arrangement effectively suppresses yaw moments induced by asymmetric pressure distributions, thus maintaining good directional stability.

Fig. 13 shows the longitudinal and lateral distances from the leader to each follower, with references (black dashed) and actual values. As speed increases, the top layer optimizer extends the longitudinal offsets: $S_{L,2}$ peaks at about 1.5 m and $S_{L,3}$ approaches 2.8 m. Lateral offsets remain moderate ($\approx$ 0.6 m and 1.2 m) to align with Kelvin wave crests/troughs and avoid the strong suction effects observed in parallel formations. In the deceleration phase, both longitudinal and lateral distances return smoothly to their initial values without noticeable overshoot.

Fig. 14 shows the total energy consumption percentage index $\%EC$ alongside the longitudinal and lateral tracking errors of both followers. In the medium high speed interval ($\approx$ 120–240 s), $\%EC$ drops below zero, reaching a minimum of about −6%, indicating a net energy saving effect. During this phase, the lateral errors increase slightly but remain within acceptable bounds. At low speeds, $\%EC$ returns to near zero or slightly positive values, as the top layer priorities compact structure and tracking accuracy over energy optimization. Overall, the echelon achieves greater energy savings than the triangular formation in medium high speed conditions, with peak savings comparable to or slightly better than the platooning case, while maintaining superior yaw stability compared to the latter.

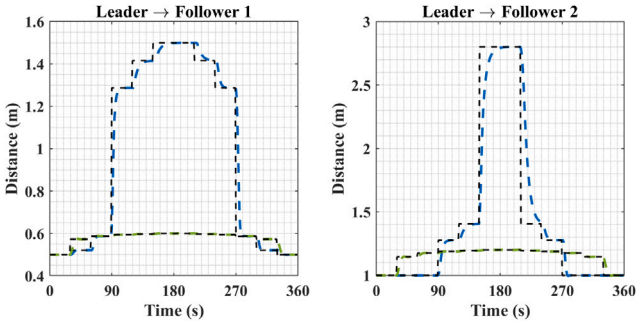

Fig. 13. Tracking performance of inter ship distances in the echelon formation. **Black**: reference distance, **Blue**: actual longitudinal distance, **Green**: actual lateral distance.

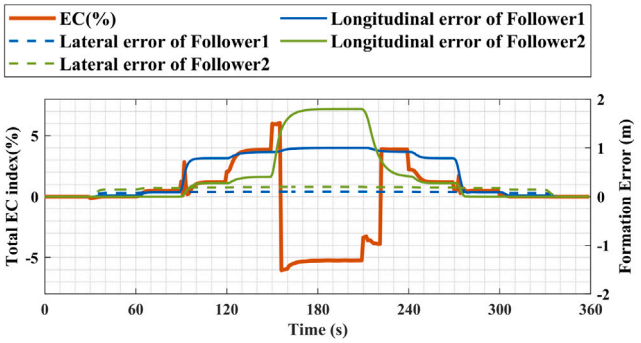

Fig. 14. Energy consumption index and formation tracking errors over time.

4.4. Experiment IV: Free formation

The final experiment investigates the optimal multi-vessel behavior under varying speeds when no explicit formation-geometry constraints are imposed. Unlike the previous experiments, which examine predefined configurations and their energy-tracking trade-offs, this study focuses on how the decision layer optimization allocates relative positions based solely on the control objective.

The control objective here is not to minimize energy consumption alone, but to achieve an optimal balance between vessel tracking performance, hydrodynamic interaction effects, and control effort. The top layer cost function retains the weighted energy and tracking terms, but no fixed reference formation offsets or relative position constraints are enforced, except for a minimal safety separation:

$$D_{ij} \geq D_{\min} = 0.3\,\text{m}, \quad \forall\, i \neq j, \tag{26}$$

to prevent vessel overlap. The speed profile is identical to the previous experiments, allowing for direct comparison of optimization behavior across different Froude number regimes.

As shown in Fig. 15, the formation evolves dynamically under the unconstrained scenario, adapting to different velocity regimes. During the medium to high speed intervals, the formation naturally transitions into an asymmetric echelon structure, where the two follower vessels are positioned on either side of the leader with slight longitudinal offsets. This echelon layout effectively avoids high resistance zones such as the turbulent wake core and destructive Kelvin wave interference regions, thus achieving optimal energy savings during this period.

At lower speeds, the system tends to adopt a more compact, nearly triangular configuration in which the vessels maintain relatively balanced positions. This layout offers enhanced tracking stability with

acceptable energy consumption, consistent with the findings of Experiments II and III.

The corresponding surge, sway, and yaw responses are shown in Fig. 16. The longitudinal speeds of all three vessels closely follow the reference profile, while lateral velocities remain small and yaw rates exhibit only moderate oscillations. This confirms that the free-formation controller maintains dynamically synchronized motion and acceptable stability, even as the layout adapts to changing speed regimes.

Fig. 17 shows that even though the optimizer is free to reshape the formation, the inter-ship distances remain within the prescribed safety bounds and vary smoothly across acceleration, cruising, and deceleration phases. This indicates that the decision layer can adjust spacing for energy benefits without sacrificing basic cohesion and collision avoidance.

As illustrated in Fig. 18, the energy consumption index ($\%EC$) exhibits significant dynamic variation throughout the simulation period. In the early stages (0–60 s), when the reference speed is relatively low, the optimizer sacrifices some consistency in relative positioning to achieve smoother velocity responses and reduced control effort. The energy index fluctuates around zero, occasionally becoming negative during high speed phases, indicating incidental energy savings driven by advantageous positioning rather than a targeted energy minimization strategy.

Between 90 s and 270 s, the reference speed increases to its peak. During this phase, the formation adaptively reshapes into an echelon structure, as shown in the trajectory and distance plots. Correspondingly, the energy saving index drops below zero, reaching as low as −5%. This negative $\%EC$ clearly reflects a net energy saving effect, primarily due to wake alignment, reduced wave making resistance, and constructive Kelvin wave interference. This result confirms the controller's ability to exploit hydrodynamic interaction for efficiency in high speed regimes.

In the deceleration phase (270–360 s), as the speed decreases, the system gradually transitions back toward a more symmetric structure. The energy index trends upward again toward 0, indicating the diminishing benefit of wave based interference exploitation. Importantly, the lateral and longitudinal formation errors remain low, suggesting that the system maintains high tracking fidelity without sacrificing control precision for energy efficiency.

Taken together, the four experiments show that the proposed hierarchical, hydrodynamics-aware control framework can (i) recover meaningful energy savings in close-spaced formations, especially at medium-to-high speeds; (ii) preserve safe inter-vessel distances and acceptable formation accuracy; and (iii) adapt the layout to operating conditions, favoring echelon-like structures at higher Froude numbers and more symmetric triangular layouts at lower speeds. These trend-level insights complement the qualitative discussion in previous sections and support the use of simple, Kelvin-wave inspired interaction models inside an MPC-based decision and control architecture.

5. Conclusion and future work

This paper has presented a hierarchical MPC framework for energy efficient formation control of multi-vessel systems, explicitly incorporating ship to ship hydrodynamic interactions. By embedding a three degree of freedom interaction model into the cost function, the supervisory controller adaptively optimizes inter ship spacing and formation geometry across different speed regimes, while the lower level MPC ensures robust trajectory tracking and stability.

Four simulation studies were conducted to assess the proposed approach. For prescribed formations, the platooning case served as a reference to illustrate how the controller enlarges longitudinal spacings at higher speeds while preserving tight lateral alignment. The triangular formation provided a balanced trade-off between energy efficiency and tracking accuracy, with smoother yaw behavior due to its symmetric layout. The echelon formation achieved the largest energy

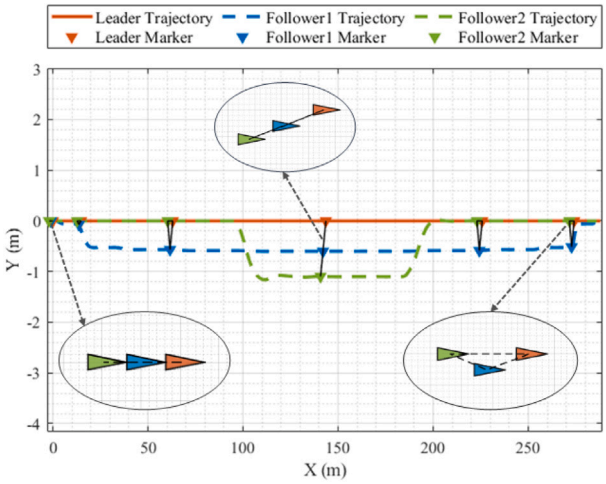

Fig. 15. The trajectories of three ASVs under triangular formation.

reductions in the medium-to-high-speed regime, with net savings of up to about 5%–6% relative to a solo-sailing baseline, while maintaining acceptable tracking errors and safety margins. In the free-formation scenario, where no layout was imposed, the optimizer autonomously steered the fleet toward an echelon-like structure at higher Froude numbers and a more symmetric, triangular-like arrangement at lower speeds. Together, these results demonstrate that simple, physically motivated interaction models can be used inside a model-based controller to recover meaningful energy savings in close-spaced formations without sacrificing basic stability or safety.

The main strengths of the proposed framework are threefold. First, it bridges hydrodynamic interaction modeling and real-time cooperative control by feeding an interaction-aware energy estimate directly into the formation decision layer, rather than treating ship-to-ship interaction solely as disturbances or offline corrections. Second, the hierarchical architecture separates slow configuration decisions from fast trajectory tracking, keeping the supervisory optimization low-dimensional while preserving the constraint-handling capabilities of MPC at the vessel level. Third, the Froude-dependent weighting mechanism allows the controller to shift emphasis between formation keeping and energy saving as operating conditions change, leading to speed-adaptive spacing and layout choices that are consistent with known hydrodynamic trends.

At the same time, several limitations must be acknowledged. The interaction model is reduced-order and tuned to reproduce qualitative resistance trends, not to predict exact loads for a specific hull; the reported energy savings should therefore be interpreted at trend level. All results are obtained from three-vessel simulations in calm water, without explicit modeling of wind, current, waves, communication delays or sensor noise, and without other traffic participants. The control architecture is centralized, and scalability to larger fleets is assessed only at the level of computational complexity, not by direct multi-dozen-vessel simulations. Finally, safety has been addressed through minimum-distance constraints and formation envelopes, but full compliance with traffic regulations has not yet been enforced.

These limitations motivate several directions for future work. First, extending the framework to distributed or decentralized MPC architectures would improve scalability and robustness in larger fleets and reduce reliance on a single coordinator. Second, coupling the proposed strategy with higher-fidelity CFD data and, ultimately, model-scale or full-scale experiments would allow quantitative validation of the interaction model and of the achievable energy savings under realistic hydrodynamic conditions. Third, integrating environmental disturbances, weather routing, and heterogeneous propulsion systems

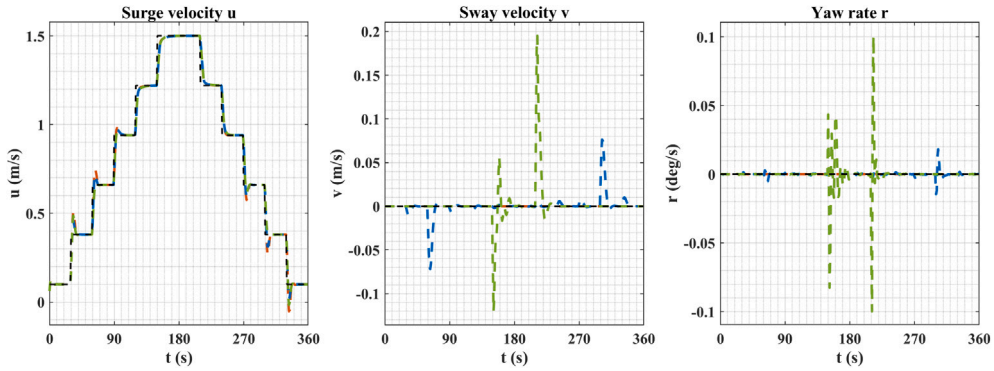

Fig. 16. Velocity response of the leader and followers. **Black**: reference trajectory, **Orange**: leader, **Blue**: follower 1, **Green**: follower 2.

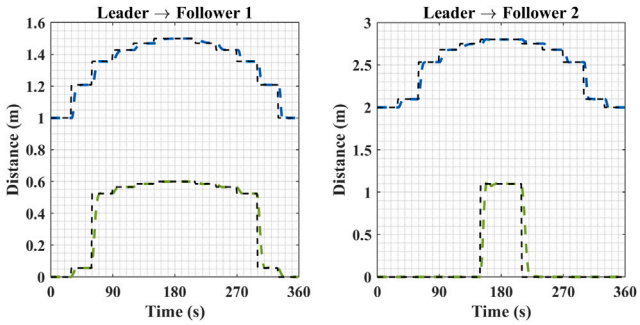

Fig. 17. Tracking performance of inter ship distances in the triangular formation. **Black**: reference distance, **Blue**: actual longitudinal distance, **Green**: actual lateral distance.

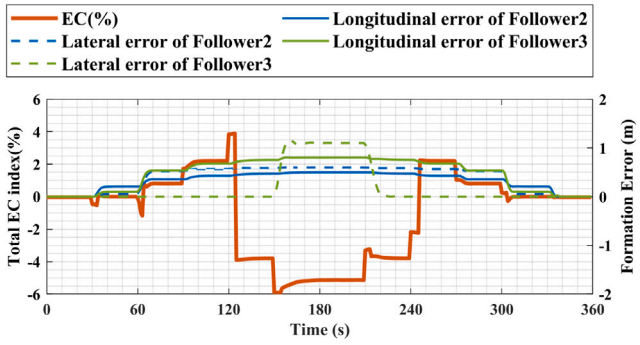

Fig. 18. Energy consumption index and formation tracking errors over time.

into the optimization could support more comprehensive energy-aware voyage planning. Finally, explicit encoding of COLREGs and traffic-safety constraints, as well as interaction with conventional vessels in mixed traffic, will be essential steps toward deploying hydrodynamics-aware, energy-conscious formation control in real inland and coastal waterways.

CRediT authorship contribution statement

Xin Xiong: Writing – original draft, Visualization, Software, Methodology, Investigation, Conceptualization. **Rudy R. Negenborn:** Writing – review & editing, Supervision, Project administration, Conceptualization. **Yusong Pang:** Writing – review & editing, Supervision, Project administration, Methodology, Conceptualization.

Declaration of competing interest

The authors declare that they have no known competing financial interests or personal relationships that could have appeared to influence the work reported in this paper.

Acknowledgments

This research is supported by the Researchlab Autonomous Shipping (RAS) of Delft University of Technology and by the China Scholarship Council under Grant 202106950062.

References

Almeida, J., Silvestre, C., Pascoal, A., 2010. Cooperative control of multiple surface vessels in the presence of ocean currents and parametric model uncertainty. Internat. J. Robust Nonlinear Control 20 (14), 1549–1565. http://dx.doi.org/10.1002/rnc.1526.

Andersson, M., Wallander, J., 2004. Kin selection and reciprocity in flight formation? Behav. Ecol. 15 (1), 158–162.

Barone, G., Buonomano, A., Del Papa, G., Maka, R., Palombo, A., 2024. Approaching zero emissions in ports: implementation of batteries and supercapacitors with smart energy management in hybrid ships. Energy Convers. Manage. 314, 118446. http://dx.doi.org/10.1016/j.enconman.2024.118446.

Chen, J., Fei, Y., Wan, Z., 2019. The relationship between the development of global maritime fleets and GHG emission from shipping. J. Environ. Manag. 242, 31–39. http://dx.doi.org/10.1016/j.jenvman.2019.03.136.

Chen, L., Hopman, H., Negenborn, R.R., 2018. Distributed model predictive control for vessel train formations of cooperative multi-vessel systems. Transp. Res. Part C: Emerg. Technol. 92, 101–118. http://dx.doi.org/10.1016/j.trc.2018.04.013.

Dai, S.L., He, S., Ma, Y., Yuan, C., 2021. Cooperative learning-based formation control of autonomous marine surface vessels with prescribed performance. IEEE Trans. Syst. Man, Cybern.: Syst. 52 (4), 2565–2577. http://dx.doi.org/10.1109/TSMC.2021.3051335.

Dean, R.G., Dalrymple, R.A., 1991. Water Wave Mechanics for Engineers and Scientists. World Scientific, Singapore.

Dong, Z., Liang, X., Guan, X., Li, W., 2022b. Formation optimization of various spacing configurations for a fleet of unmanned surface vehicles based on a hydrodynamic energy-saving strategy. Ocean Eng. 266, 112824. http://dx.doi.org/10.1016/j.oceaneng.2022.112824.

Dong, Z., Qi, S., Yu, M., Zhang, Z., Zhang, H., Li, J., Liu, Y., 2022c. An improved dynamic surface sliding mode method for autonomous cooperative formation control of underactuated USVs with complex marine environment disturbances. Pol. Marit. Res. 29 (2), 34–45. http://dx.doi.org/10.2478/pomr-2022-0025.

Dong, K., Wang, X., Zhang, D., Liu, L., Feng, D., 2022a. CFD research on the hydrodynamic performance of submarine sailing near the free surface with long-crested waves. J. Mar. Sci. Eng. 10 (1), 90. http://dx.doi.org/10.3390/jmse10010090.

Du, Z., Reppa, V., Negenborn, R.R., 2021. MPC-based COLREGS compliant collision avoidance for a multi-vessel ship-towing system. In: 2021 European Control Conference. ECC, IEEE, pp. 1857–1862. http://dx.doi.org/10.23919/ECC54610.2021.9655091.

Fang, Z., Jiang, D., Huang, J., Cheng, C., Sha, Q., He, B., Li, G., 2022. Autonomous underwater vehicle formation control and obstacle avoidance using multi-agent generative adversarial imitation learning. Ocean Eng. 262, 112182. http://dx.doi.org/10.1016/j.oceaneng.2022.112182.

Fossen, T.I., 2011. Handbook of Marine Craft Hydrodynamics and Motion Control. John Wiley & Sons, Chichester, UK.

Hagen, I.B., Kufoalor, D., Johansen, T.A., Brekke, E.F., 2022. Scenario-based model predictive control with several steps for colregs compliant ship collision avoidance. IFAC-PapersOnLine 55 (31), 307–312. http://dx.doi.org/10.1016/j.ifacol.2022.10.447.

Haseltalab, A., Negenborn, R.R., 2019. Model predictive maneuvering control and energy management for all-electric autonomous ships. Appl. Energy 251, 113308. http://dx.doi.org/10.1016/j.apenergy.2019.113308.

He, Z., Liu, C., Chu, X., Negenborn, R.R., Wu, Q., 2022b. Dynamic anti-collision A-star algorithm for multi-ship encounter situations. Appl. Ocean Res. 118, 102995. http://dx.doi.org/10.1016/j.apor.2021.102995.

He, Y., Mou, J., Chen, L., Zeng, Q., Huang, Y., Chen, P., Zhang, S., 2022a. Will sailing in formation reduce energy consumption? Numerical prediction of resistance for ships in different formation configurations. Appl. Energy 312, 118695. http://dx.doi.org/10.1016/j.apenergy.2022.118695.

Hong, S.H., Kim, D.M., Kim, S.J., 2024. Power control strategy optimization to improve energy efficiency of the hybrid electric propulsion ship. IEEE Access 12, 22534–22545. http://dx.doi.org/10.1109/ACCESS.2024.3364374.

International Towing Tank Conference, 1957. ITTC 1957 Performance Prediction Method. Technical Report, ITTC Resistance Committee.

Karatuğ, c., Tadros, M., Ventura, M., Soares, C.G., 2024. Decision support system for ship energy efficiency management based on an optimization model. Energy 292, 130318. http://dx.doi.org/10.1016/j.energy.2024.130318.

Li, L., Nagy, M., Graving, J.M., Bak-Coleman, J., Xie, G., Couzin, I.D., 2020. Vortex phase matching as a strategy for schooling in robots and in fish. Nat. Commun. 11 (1), 5408.

Li, X., Sun, B., Jin, J., Ding, J., 2023. Ship speed optimization method combining Fisher optimal segmentation principle. Appl. Ocean Res. 140, 103743. http://dx.doi.org/10.1016/j.apor.2023.103743.

Liang, X., Zhang, Y., Yang, G., 2021. Platoon control design for unmanned surface vehicles subject to input delay. Sci. Rep. 11 (1), 1481. http://dx.doi.org/10.1038/s41598-020-80348-4.

Liu, Y., Bucknall, R., 2015. Path planning algorithm for unmanned surface vehicle formations in a practical maritime environment. Ocean Eng. 97, 126–144. http://dx.doi.org/10.1016/j.oceaneng.2015.01.008.

Liu, C., Hu, Q., Wang, X., 2021a. Distributed guidance-based formation control of marine vehicles under switching topology. Appl. Ocean Res. 106, 102465.

Liu, C., Qi, J., Chu, X., Zheng, M., He, W., 2021b. Cooperative ship formation system and control methods in the ship lock waterway. Ocean Eng. 226, 108826. http://dx.doi.org/10.1016/j.oceaneng.2021.108826.

Liu, L., Wang, D., Peng, Z., Li, T., 2017. Modular adaptive control for LOS-based cooperative path maneuvering of multiple underactuated autonomous surface vehicles. IEEE Trans. Syst. Man, Cybern.: Syst. 47 (7), 1613–1624. http://dx.doi.org/10.1109/TSMC.2017.2650219.

Luo, F., Wang, T., Gao, C., Rao, Z., Liu, B., 2024. Distributed formation coordinated control of multiple unmanned surface vehicles based on deep reinforcement learning. In: International Conference on Intelligent Robotics and Applications. Springer, pp. 334–348.

Lv, G., Peng, Z., Liu, L., Wang, J., 2022. Barrier-certified distributed model predictive control of under-actuated autonomous surface vehicles via neurodynamic optimization. IEEE Trans. Syst. Man, Cybern.: Syst. 53 (1), 563–575. http://dx.doi.org/10.1109/TSMC.2022.3184811.

Molland, A.F., Turnock, S.R., Hudson, D.A., 2017. Ship Resistance and Propulsion. Cambridge University Press, Cambridge.

Mwaffo, V., 2024. Formation control and collision avoidance of unmanned water surface vehicles in maritime environments. J. Franklin Inst. 361 (7), 106791.

Newman, J.N., 2018. Marine Hydrodynamics. The MIT Press.

Nguyen, V.T., Chandar, D., 2023. Ship specific optimization of pre-duct energy saving devices using reduced order models. Appl. Ocean Res. 131, 103449. http://dx.doi.org/10.1016/j.apor.2022.103449.

Peng, Z., Wang, J., Wang, D., 2017. Distributed maneuvering of autonomous surface vehicles based on neurodynamic optimization and fuzzy approximation. IEEE Trans. Control Syst. Technol. 26 (3), 1083–1090. http://dx.doi.org/10.1109/TCST.2017.2699167.

Phillips, A., Blake, J., Boyd, S., Ward, S., Griffiths, G., 2012. Nature in engineering for monitoring the oceans (NEMO): an isopycnal soft bodied approach for deep diving autonomous underwater vehicles. In: 2012 IEEE/OES Autonomous Underwater Vehicles. AUV, pp. 1–8. http://dx.doi.org/10.1109/AUV.2012.6380743.

Phillips, A., Turnock, S., Furlong, M., 2010a. The use of computational fluid dynamics to aid cost-effective hydrodynamic design of autonomous underwater vehicles. Proc. Inst. Mech. Eng. Part M: J. Eng. Marit. Environ. 224 (4), 239–254. http://dx.doi.org/10.1243/14750902JEME199.

Phillips, A.B., Turnock, S.R., Furlong, M., 2010b. Influence of turbulence closure models on the vortical flow field around a submarine body undergoing steady drift. J. Mar. Sci. Technol. 15, 201–217. http://dx.doi.org/10.1007/s00773-010-0090-1.

Rattanasiri, P., Wilson, P.A., Phillips, A.B., 2012. Numerical investigation of the drag of twin prolate spheroid hulls in various longitudinal and transverse configurations. In: 2012 IEEE/OES Autonomous Underwater Vehicles. AUV, pp. 1–7. http://dx.doi.org/10.1109/AUV.2012.6380731.

Rattanasiri, P., Wilson, P.A., Phillips, A.B., 2015. Numerical investigation of a pair of self-propelled AUVs operating in tandem. Ocean Eng. 100, 126–137. http://dx.doi.org/10.1016/j.oceaneng.2015.04.031.

Riahifard, A., Hosseini Rostami, S.M., Wang, J., Kim, H.J., 2019. Adaptive leader-follower formation control of under-actuated surface vessels with model uncertainties and input constraints. Appl. Sci. 9 (18), 3901. http://dx.doi.org/10.3390/app10072496.

Shang, W., Liu, M., Zhang, D., Zhu, H., 2023. Formation control of multiple mobile robots based on iterative learning distributed model predictive control. IEEE Access 11, 120034–120048. http://dx.doi.org/10.1109/ACCESS.2023.3312174.

Tang, Z., Wang, L., Wang, Y., He, H., Li, B., 2022. Distributed-integrated model predictive control for cooperative operation with multi-vessel systems. J. Mar. Sci. Technol. 27 (4), 1281–1301. http://dx.doi.org/10.1007/s00773-022-00905-6.

Tsolakis, A., Negenborn, R.R., Reppa, V., Ferranti, L., 2024. Model predictive trajectory optimization and control for autonomous surface vessels considering traffic rules. IEEE Trans. Intell. Transp. Syst. 25 (8), 9895–9908. http://dx.doi.org/10.1109/TITS.2024.3357284.

Vorkapić, A., Radonja, R., Martinčić-Ipšić, S., 2021. Predicting seagoing ship energy efficiency from the operational data. Sensors 21 (8), 2832.

Wang, K., Li, Z., Zhang, R., Ma, R., Huang, L., Wang, Z., Jiang, X., 2025. Computational fluid dynamics-based ship energy-saving technologies: A comprehensive review. Renew. Sustain. Energy Rev. 207, 114896.

Wang, Y., Shen, C., Huang, J., Chen, H., 2024. Model-free adaptive control for unmanned surface vessels: A literature review. Syst. Sci. Control. Eng. 12 (1), 2316170. http://dx.doi.org/10.1080/21642583.2024.2316170.

Wang, K., Yan, X., Yuan, Y., Jiang, X., Lin, X., Negenborn, R.R., 2018. Dynamic optimization of ship energy efficiency considering time-varying environmental factors. Transp. Res. Part D: Transp. Environ. 62, 685–698. http://dx.doi.org/10.1016/j.trd.2018.04.005.

Xiong, X., Negenborn, R.R., Pang, Y., 2024. Influence of ship-to-ship interaction on formation control of multi-vessel systems. In: Proceedings of the 21st International Conference on Informatics in Control, Automation and Robotics, vol. 1, pp. 25–36.

Xue, Y., Yang, C.J., Dong, X.Q., Li, W., Noblesse, F., 2022. Design of marine propellers with prescribed and optimal spanwise circulation distributions based on genetic algorithms and neural network. Appl. Ocean Res. 127, 103318. http://dx.doi.org/10.1016/j.apor.2022.103318.

Yan, R., Yang, D., Wang, T., Mo, H., Wang, S., 2024. Improving ship energy efficiency: Models, methods, and applications. Appl. Energy 368, 123132. http://dx.doi.org/10.1016/j.apenergy.2024.123132.

Yanuar, Gunawan, Sunaryo, Jamaluddin, A., 2012. Micro-bubble drag reduction on a high speed vessel model. J. Mar. Sci. Appl. 11, 301–304. http://dx.doi.org/10.1007/s11804-012-1136-z.

Yuan, Z.M., Chen, M., Jia, L., Ji, C., Incecik, A., 2021. Wave-riding and wave-passing by ducklings in formation swimming. J. Fluid Mech. 928, R2.

Zhang, G., Liu, S., Zhang, X., Zhang, W., 2022. Event-triggered cooperative formation control for autonomous surface vehicles under the maritime search operation. IEEE Trans. Intell. Transp. Syst. 23 (11), 21392–21404.

Zhao, D., Mu, J., Sun, H., Bi, M., Liu, X., 2025. Hydrodynamic interference mechanism of ships in formation navigation. Ocean Eng. 339, 122023. http://dx.doi.org/10.1016/j.oceaneng.2024.122023.

Zheng, H., Negenborn, R.R., Lodewijks, G., 2014. Trajectory tracking of autonomous vessels using model predictive control. IFAC Proc. Vol. 47 (3), 8812–8818. http://dx.doi.org/10.3182/20140824-6-ZA-1003.00767.

Zheng, H., Negenborn, R.R., Lodewijks, G., 2016. Fast ADMM for distributed model predictive control of cooperative waterborne AGVs. IEEE Trans. Control Syst. Technol. 25 (4), 1406–1413.

Zhou, X., Sutulo, S., Soares, C.G., 2015. Simulation of hydrodynamic interaction forces acting on a ship sailing across a submerged bank or an approach channel. Ocean Eng. 103, 103–113. http://dx.doi.org/10.1016/j.oceaneng.2015.04.067.